A&A 463, 937–947 (2007)
DOI: 10.1051/0004-6361:20065961

Astronomy & Astrophysics

GMRT radio halo survey in galaxy clusters at $z = 0.2$–0.4⋆

I. The REFLEX sub-sample

T. Venturi[1], S. Giacintucci[1,2,3], G. Brunetti[1], R. Cassano[1,3], S. Bardelli[2], D. Dallacasa[1,3], and G. Setti[1,3]

[1] INAF – Istituto di Radioastronomia, via Gobetti 101, 40129 Bologna, Italy
e-mail: tventuri@ira.inaf.it
[2] INAF – Osservatorio Astronomico di Bologna, via Ranzani 1, 40127 Bologna, Italy
[3] Dipartimento di Astronomia, Università di Bologna, via Ranzani 1, 40126 Bologna, Italy

Received 3 July 2006 / Accepted 7 December 2006

ABSTRACT

Aims. We present the first results of an ongoing project devoted to the search of giant radio halos in galaxy clusters located in the redshift range $z = 0.2$–0.4. One of the main goals of our study is to measure the fraction of massive galaxy clusters in this redshift interval hosting a radio halo, and to constrain the expectations of the particle re-acceleration model for the origin of non-thermal radio emission in galaxy clusters.
Methods. We selected 27 REFLEX clusters and here we present Giant Metrewave Radio Telescope (GMRT) observations at 610 MHz for 11 of them. The sensitivity (1σ) in our images is in the range 35–100 μJy beam^{-1} for all clusters.
Results. We found three new radio halos, doubling the number of halos known in the selected sample. In particular, giant radio halos were found in A 209 and RXCJ 2003.5–2323, and one halo (of smaller size) was found in RXCJ 1314.4–2515. Candidate extended emission on smaller scale was found around the central galaxy in A 3444 which deserves further investigation. Furthermore, a radio relic was found in A 521, and two relics were found in RXCJ 1314.5–2515. The remaining six clusters observed do not host extended emission of any kind.

Key words. radio continuum: galaxies – galaxies: clusters: general – radio continuum: general

1. Introduction

Radio and X-ray observations of galaxy clusters prove that thermal and non-thermal plasma components coexist in the intracluster medium (ICM). While X-ray observations reveal the presence of diffuse hot gas, the existence of extended cluster-scale radio sources in a number of galaxy clusters, well known as *radio halos* and *relics*, prove the presence of relativistic electrons and magnetic fields.

Both radio halos and relics are low surface brightness sources with steep radio spectra, whose linear size can reach and exceed the Mpc scale. Radio halos are usually located at the centre of galaxy clusters, show a fairly regular radio morphology, and lack an obvious optical counterpart. A total of about 20 radio halos have been detected up to now (Giovannini et al. 1999; Giovannini & Feretti 2002; Kempner & Sarazin 2001; Bacchi et al. 2003). Relics are usually found at the cluster periphery, their radio emission is highly polarized (up to ∼30%), and shows a variety of radio morphologies, such as sheet, arc, toroids. At present a total of ∼20 relics (including candidates) are known (Kempner & Sarazin 2001; Giovannini & Feretti 2004).

Evidence in the optical and X-ray bands has been accumulated in favour of the hierarchical formation of galaxy clusters through merging processes (for a collection of reviews on this subject see Feretti et al. 2002), and this has provided insightful pieces of information in our understanding of radio halos. It is not clear whether all clusters with signatures of merging processes also possess a radio halo; on the other hand, all clusters hosting a radio halo show sub-structures in the X-ray emission, and the most powerful radio halos are hosted in clusters which most strongly depart from virialization (Buote 2001). Giovannini et al. (1999) showed that in the redshift interval 0–0.2 the detection rate of cluster radio halos increases with increasing X-ray luminosity, which suggests a connection with the gas temperature and cluster mass.

The very large extent of radio halos poses the question of their origin, since the diffusion time the relativistic electrons need to cover the observed Mpc size is 30–100 times longer than their radiative lifetime. Two main possibilities have been investigated so far: "primary models", in which particles are in-situ re-accelerated in the ICM, and "secondary models" in which the emitting electrons are secondary products of hadronic collisions in the ICM (for reviews on these models see Blasi 2004; Brunetti 2003, 2004; Ensslin 2004; Feretti 2003; Hwang 2004; Sarazin 2002). Cluster mergers are among the most energetic events in the Universe, with an energy release up to 10^{64} erg, and a challenging question is if at least a fraction of such energy may be channelled into particle reacceleration (e.g. Tribble 1993). Indeed observational support (for a review see Feretti 2003) is now given to the particle re-acceleration model, which assumes that the radiating electrons are stochastically re-accelerated by turbulence in the ICM and that the bulk of this turbulence is injected during cluster mergers (Brunetti et al. 2001; Petrosian 2001; Fujita et al. 2003; Brunetti et al. 2004).

Although the physics of particle re-acceleration by turbulence has been investigated in some detail and the model expectations seem to reproduce the observed radio features,

⋆ Figures A1 to A10 are only available in electronic form at http://www.aanda.org

only recently statistical calculations in the framework of the re-acceleration model have been carried out by Cassano & Brunetti (2005, hereinafter CB05). Making use of semi-analytical calculations they estimated the energy of turbulence injected in galaxy clusters through cluster mergers, and derived the expected occurrence of *giant*[1] radio halos as a function of the mass and dynamical status of the clusters in the framework of the merger-induced particle re-acceleration scenario.

The most relevant result of those calculations is that the occurrence of giant radio halos increases with the cluster mass. Furthermore, the expected fration of clusters with giant radio halos at $z \leq 0.2$ can be reconciled with the observed one (Giovannini et al. 1999) for viable values of the model parameters.

Cassano et al. (2004, hereinafter CBS04) and Cassano et al. (2006, hereinafter CBS06) showed that the bulk of giant radio halos are expected in the redshift range $z \sim 0.2 \div 0.4$ as a result of two competing effects, i.e. the decrease of the fraction of clusters with halos in a given mass range and the increase of the volume of the Universe with increasing redshift. Given that inverse Compton losses increase with the redshift, it is expected that powerful giant radio halos at $z > 0.2$ are preferentially found in massive clusters ($M \sim 2$–$3 \times 10^{15}\ M_{\odot}$) undergoing merging events. In particular, it is expected that a fraction of 10–35% of clusters in this redshift interval and mass range may host a giant radio halo.

With the aim to investigate the connection between cluster mergers and the presence of cluster-type radio sources, in particular to derive the fraction of massive galaxy clusters in the range $0.2 < z < 0.4$ hosting a radio halo and constrain the predictions of the re-acceleration model in the same redshift interval, we undertook an observational study using the Giant Metrewave Radio Telescope (GMRT, Pune, India) at 610 MHz. Our project will be presented here and in future papers, and will be referred to as the GMRT Radio Halos Survey.

Here we report the results on 11 galaxy clusters observed with the GMRT in January 2005. The paper is organised as follows: in Sect. 2 we present the sample of galaxy clusters; the radio observations are described in Sect. 3; the analysis of our results and a brief discussion are given in Sects. 4 and 5 respectively.

2. The cluster sample

In order to obtain a statistically significant sample of clusters suitable for our aims, we based our selection on the ROSAT-ESO Flux Limited X-ray (REFLEX) galaxy cluster catalogue (Böhringer et al. 2004) and on the extended ROSAT Brightest Cluster Sample (BCS) catalogue (Ebeling et al. 1998, 2000). Here we will concentrate on the REFLEX sample, which was observed with the GMRT in January 2005 (present paper, see next section), in October 2005 and August 2006 (Venturi et al., in preparation).

From the REFLEX catalogue we selected all clusters satisfying the following criteria:

1) $L_{\rm X}(0.1\text{–}2.4\ {\rm keV}) > 5 \times 10^{44}\ {\rm erg\,s^{-1}}$;
2) $0.2 < z < 0.4$;
3) $-30^{\circ} < \delta < +2.5^{\circ}$.

[1] Linear size $\geq$1 Mpc as defined in CB05, with $H_0 = 50\ {\rm km\,s^{-1}\,Mpc^{-1}}$. This size corresponds to $\gtrsim$700 kpc with the cosmology assumed in this paper, i.e. $H_0 = 70\ {\rm km\,s^{-1}\,Mpc^{-1}}$, $\Omega_{\rm m} = 0.3$ and $\Omega_{\Lambda} = 0.7$.

The lower limit of $\delta = -30^{\circ}$ was chosen in order to ensure a good u-v coverage with the GMRT, while the value of $\delta = +2.5^{\circ}$ is the REFLEX upper limit.

The limit in X-ray luminosity is aimed at selecting massive clusters, which are expected to host giant radio halos (CBS04, CB05 and references therein). It corresponds to a lower limit in the virial mass of $M_{\rm V} > 1.4 \times 10^{15}\ M_{\odot}$ if the $L_{\rm X}$–$M_{\rm V}$ derived in CBS06 is assumed. We point out that the $L_{\rm X}$–$M_{\rm V}$ correlation in CBS06 has a statistical dispersion of ~30%. This error dominates over the systematic additional uncertainty introduced by the fact that the correlation was obtained using the $z < 0.2$ cluster sample in Reiprich & Böhringer (2002).

We obtained a total of 27 clusters. The source list is reported in Table 1, where we give (1) the REFLEX name, (2) alternative name from other catalogues, (3) and (4) J2000 coordinates, (5) redshift, (6) the X-ray luminosity in the 0.1–2.4 keV band, (7) and (8) estimates for the virial mass $M_{\rm V}$ and virial radius $R_{\rm V}$ respectively (from the $L_{\rm X}$–$M_{\rm V}$ correlation derived in CBS06).

The location of the 27 clusters of the sample in the $L_{\rm X} - z$ plane for the whole REFLEX catalogue is reported in Fig. 1.

3. Radio observations

From the sample given in Table 1 we selected all clusters with no radio information available in the literature at the time our GMRT proposal was written. We also excluded all clusters belonging to the GMRT Cluster Key Project (P.I. Kulkarni), and remained with a total of 18 clusters, marked with the symbol $\surd$ in Table 1.

From the list of marked clusters, 11 were given higher priority and were observed with the GMRT during a 27-h run allocated in January 2005. Table 2 reports the following information: cluster name, half power beamwidth (HPWB) of the full array of the observations (arcsec), total time on source (minutes) and rms (1σ in $\mu{\rm Jy\,b^{-1}}$) in the full resolution image.

Five clusters listed in Table 1 were observed with the GMRT in a second observing run carried out in October 2005, i.e. A 2813, A 2485, A 2895, RXCJ 1115.8+0129 and RXCJ 1512.2–2254; finally the two remaining clusters A 2645 and A 2667 will be observed in August 2006. They will all be presented in a future paper (Venturi et al., in preparation).

The observations were carried out at 610 MHz, using simultaneously two 16 MHz bands (upper side band, USB, and lower side band, LSB), for a total of 32 MHz. Left and right polarization were recorded for each band. The observations were carried out in spectral line mode, with 128 channels each band, and a spectral resolution of 125 kHz/channel. The data reduction and analysis were carried out with the NRAO Astronomical Image Processing System (AIPS) package. In order to reduce the size of the dataset, after bandpass calibration the central 94 channels were averaged to 6 channels of ~2 MHz each. For each source the USB and LSB datasets, as well as the datasets taken in different days, were calibrated and reduced separately, then the final images from each individual dataset were combined in the image plane to obtain the final image. Wide-field imaging was adopted in each step of the data reduction.

For each cluster we produced images over a wide range of resolutions, in order to fully exploit the information GMRT can provide. We point out that the nominal largest detectable structure provided by the GMRT at 610 MHz is 17′. This value ensures the possible detection of the extended radio sources we are searching for, since the angular scale covered by a 1 Mpc-size structure is ~5′ at $z = 0.2$ and ~3′ at $z = 0.4$.

Table 1. Cluster sample from the REFLEX catalogue.

REFLEX Name	Alt. name	RA_{J2000}	Dec_{J2000}	z	$L_X(0.1\text{–}2.4\ keV)$ 10^{44} erg s^{-1}	M_V 10^{15} $M_\odot$	R_V Mpc
√ RXCJ 0003.1−0605	A 2697	00 03 11.8	−06 05 10	0.2320	6.876	1.68	2.70
⋆ RXCJ 0014.3−3023	A 2744	00 14 18.8	−30 23 00	0.3066	12.916	2.58	2.99
√ RXCJ 0043.4−2037	A 2813	00 43 24.4	−20 37 17	0.2924	7.615	1.80	2.67
√ RXCJ 0105.5−2439	A 141	01 05 34.8	−24 39 17	0.2300	5.762	1.50	2.60
√ RXCJ 0118.1−2658	A 2895	01 18 11.1	−26 58 23	0.2275	5.559	1.45	2.58
√ RXCJ 0131.8−1336	A 209	01 31 53.0	−13 36 34	0.2060	6.289	1.58	2.69
√ RXCJ 0307.0−2840	A 3088	03 07 04.1	−28 40 14	0.2537	6.953	1.69	2.67
RXCJ 0437.1+0043	–	04 37 10.1	+00 43 38	0.2842	8.989	2.02	2.79
√ RXCJ 0454.1−1014	A 521	04 54 09.1	−10 14 19	0.2475	8.178	1.89	2.78
RXCJ 0510.7−0801	–	05 10 44.7	−08 01 06	0.2195	8.551	1.95	2.86
√ RXCJ 1023.8−2715	A 3444	10 23 50.8	−27 15 31	0.2542	13.760	2.69	3.12
√ RXCJ 1115.8+0129	–	11 15 54.0	+01 29 44	0.3499	13.579	2.67	2.95
⋆ RXCJ 1131.9−1955	A 1300	11 31 56.3	−19 55 37	0.3075	13.968	2.72	3.04
RXCJ 1212.3−1816	–	12 12 18.9	−18 16 43	0.2690	6.197	1.56	2.58
√ RXCJ 1314.4−2515	–	13 14 28.0	−25 15 41	0.2439	10.943	2.30	2.98
√ RXCJ 1459.4−1811	S 780	14 59 29.3	−18 11 13	0.2357	15.531	2.92	3.24
RXCJ 1504.1−0248	–	15 04 07.7	−02 48 18	0.2153	28.073	4.37	3.75
√ RXCJ 1512.2−2254	–	15 12 12.6	−22 54 59	0.3152	10.186	2.19	2.81
RXCJ 1514.9−1523	–	15 14 58.0	−15 23 10	0.2226	7.160	1.73	2.74
⋆ RXCJ 1615.7−0608	A 2163	16 15 46.9	−06 08 45	0.2030	23.170	3.84	3.62
√ RXCJ 2003.5−2323	–	20 03 30.4	−23 23 05	0.3171	9.248	2.05	2.75
RXCJ 2211.7−0350	–	22 11 43.4	−03 50 07	0.2700	7.418	1.77	2.69
√ RXCJ 2248.5−1606	A 2485	22 48 32.9	−16 06 23	0.2472	5.100	1.37	2.50
√ RXCJ 2308.3−0211	A 2537	23 08 23.2	−02 11 31	0.2966	10.174	2.19	2.85
√ RXCJ 2337.6+0016	A 2631	23 37 40.6	+00 16 36	0.2779	7.571	1.79	2.69
√ RXCJ 2341.2−0901	A 2645	23 41 16.8	−09 01 39	0.2510	5.789	1.49	2.57
√ RXCJ 2351.6−2605	A 2667	23 51 40.7	−26 05 01	0.2264	13.651	2.68	3.16

Symbols are as follows: √ marks the clusters observed by us with the GMRT as part of our radio halo survey; ⋆ marks the clusters with radio halo known from the literature (A 2744 Govoni et al. 2001; A 1300 Reid et al. 1999; A 2163 Herbig & Birkinshaw 1994; and Feretti et al. 2001). All the remaining clusters are part of the GMRT cluster Key Project (P.I. Kulkarni).

The sensitivity of our observations (1σ level) is in the range 35–100 μJy for the full resolution images (see Table 2), which were obtained by means of uniform weighting. The spread in the noise level depends most critically on the total time on source, on the total bandwidth available (in few cases only one portion of the band provided useful data, see individual clusters in Sect. 4), and on the presence of strong sources in the imaged field. Slightly lower values for the noise level are obtained for the low resolution images (see Sect. 4 and figure captions), which were made using natural weighting.

The average residual amplitude errors in our data are of the order of $\lesssim$5%.

4. Results

Cluster scale radio emission either in the form of radio halo or relic was detected in 4 clusters of the sample (Sect. 4.1); in one cluster extended emission was found around the dominant galaxy (Sect. 4.2); for the remaining six clusters no hint of extended emission is present at the sensitivity level of the observations (Sect. 4.3). Details on each cluster are given in this section. In Appendix A we report the 610 MHz radio contours within the virial radius for all the observed clusters. All the images were convolved with a HPWB of $15.0'' \times 12.0''$, except for A 209, RXCJ 1314.4–2515 and RXCJ 2003.5–2323 where a different resolution was chosen in order to complement the information provided in Figs. 2–6. Table 3 reports the observational information for the detected cluster-scale radio sources. The last column in the table, L_1/L_2, provides the ratio between the major (LAS) and minor axis of the extended emission. The linear size and flux densities were derived from the 3σ contour level.

4.1. Clusters with halos, giant halos and relics

4.1.1. Abell 209

Abell 209 (RXCJ 0131.8–1336) is a richness $R = 3$ cluster at $z = 0.2060$ ($1'' = 3.377$ kpc). A high X-ray temperature is reported in the literature. Rizza et al. (1998) estimated a mean gas temperature of $kT \sim 10$ keV from the ROSAT X-ray luminosity; this value was confirmed by Mercurio et al. (2004a) from the analysis of *Chandra* archive data.

The cluster has been extensively studied at optical (Mercurio et al. 2003, 2004a,b; Haines et al. 2004), and X-ray wavelenghts (ROSAT–HRI, Rizza et al. 1998; Mercurio et al. 2004a). These studies show that A 209 is far from a relaxed dynamical stage, and it is undergoing a strong dynamical evolution. In particular the X-ray and the optical data suggest that A 209 is experiencing a merging event between two or more components.

Mercurio et al. (2003) provided an estimate of the virial mass of the cluster, $M_V = 2.25^{+0.63}_{-0.65} \times 10^{15}\ M_\odot$, consistent with our estimate given in Table 1 if we account for the uncertainty of our value (see Sect. 2).

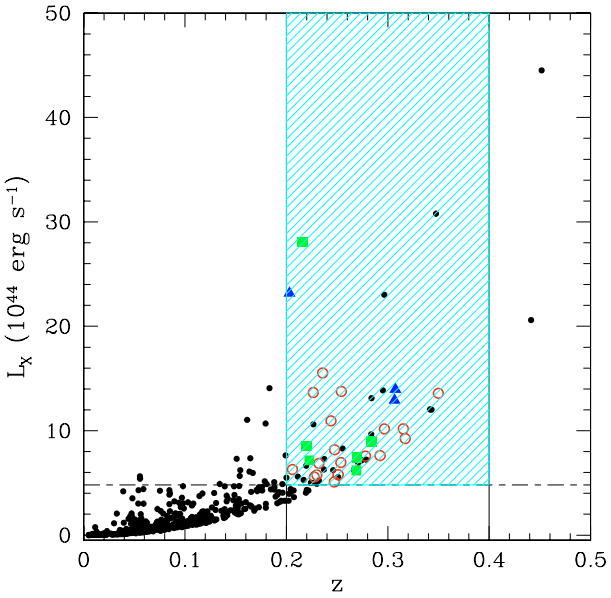

Fig. 1. L_x–z plot (0.1–2.4 keV) for the REFLEX clusters. Open red circles show the clusters selected for the GMRT observations of the present project (marked with the symbol √ in Table 1; see Sect. 3 for details); filled blue triangles indicate those clusters (marked with ⋆ in Table 1) which are known to host a radio halo from the literature, i.e. A 2744 (Govoni et al. 2001), A 1300 (Reid et al. 1999) and A 2163 (Herbig & Birkinshaw 1994; Feretti et al. 2001); filled green squares indicate the clusters of the sample belonging to the GMRT Cluster Key Project (P.I. Kulkarni). The light blue dashed region is the one surveyed in our project.

The cluster merging scenario is confirmed by the weak lensing analysis carried out by Dahle et al. (2002), who found two significant peaks in the mass distribution of the cluster: the largest one is close to the central cD galaxy, and the secondary mass peak is located at about 5 arcmin north of the cluster centre and associated to a peak in the optical galaxy distribution.

610 MHz contours of the A 209 emission within the virial radius are given in Fig. A.1, while Fig. 2 shows the central part of the field at two different resolutions superposed on the POSS-2 image. Inspection of Fig. A.1 and of the right panel in Fig. 2 coupled with flux density measurements, suggests the presence of extended emission around the individual central cluster radio galaxies.

In order to highlight such emission we subtracted all the individual sources visible in the full resolution image from the $u - v$ data, and convolved the residuals with a HPBW with size $32.0'' \times 30.0''$. The image is reported in Fig. 3.

The adopted procedure indeed confirms the existence of cluster scale extended emission. The possible presence of a radio halo in A 209 was suggested by Giovannini et al. (1999) from inspection of the NRAO VLA Sky Survey (NVSS), and confirmed in Giovannini et al. (2006) on the basis of 1.4 GHz VLA observations. Our GMRT image in Fig. 3 is in partial agreement with the size and morphology of the VLA 1.4 GHz image shown by those authors. The largest angular size (LAS) is ∼4′, i.e. ∼810 kpc, therefore we classify the source as a *giant* radio halo. Its total flux density, measured after subtraction of the individual radio sources (see left panel of Fig. 2) is $S_{610\,\mathrm{MHz}} = 24.0 \pm 3.6$ mJy, which implies a total radio power of $\log P_{610\,\mathrm{MHz}}$ (W/Hz) = 24.46. The difficulty in subtracting the extended individual sources (in particular the head-tail radio galaxy located just South of the cluster centre) reflects both in the large error associated with the flux density measurement, and in the unusual brightness distribution of the radio halo, characterised by two peaks of emission.

Further observations are already in progress with the GMRT, in order to better image and study this source.

Table 2. GMRT observations.

Cluster	Beam, PA (full array) "×", °	Obs. time min	rms μJy b^{-1}
A 2697	8.5 × 5.0, –83	90	80
A 141	7.7 × 7.4, 75	150	100
A 209	8.0 × 5.0, 64	240	60
A 3088	8.0 × 7.0, 40	190	65
A 521	8.6 × 4.0, 57	210	35
A 3444	7.6 × 4.9, 19	120	67
RXCJ 1314.4–2515	8.0 × 5.0, 15	150	65
S 780	7.5 × 5.0, 25	80	70
RXCJ 2003.5–2323	6.9 × 5.0, –3	240	40
A 2537	10.3 × 6.0, 67	150	60
A 2631	9.2 × 6.3, –77	240	50

4.1.2. Abell 521

A detailed study of A 521 (RXCJ 0454.1–1014, $z = 0.2475$, $1'' = 3.875$ kpc) has already been published by Giacintucci et al. (2006). This merging cluster hosts a radio relic located at the border of the X-ray emission. We discussed the origin of this source in the light of current scenarios for the formation of radio relics, i.e. acceleration of electrons from the thermal pool or compression of fossil radio plasma, both through merger shock waves. We refer to that paper for the images and radio information and will include A 521 in the discussion in Sect. 5. All values and observational parameters reported in Tables 2 and 3 are taken from Giacintucci et al. (2006).

4.1.3. RXCJ 1314.4–2515

Evidence of a disturbed dynamical status for the cluster RXCJ 1314.4–2515 ($z = 0.2439$, $1'' = 3.806$ kpc) is reported in the literature. The redshift distribution of the cluster galaxies clearly shows a bimodal structure, with two peaks separated in velocity space by ∼1700 km s^{-1} (Valtchanov et al. 2002). The X-ray morphology of the cluster is also bimodal, and it is elongated along the E-W direction, the western peak being the brightest (Valtchanov et al. 2002).

This cluster was observed with the VLA at 1.4 GHz by Feretti et al. (2005), who revealed the presence of a radio halo at the cluster centre and two peripheral sources, which they classified as relics.

Figure A.2 reports the contour image of our 610 MHz observations at the resolution of $15.0'' \times 13.0''$ within the virial radius. The central part of the cluster is given in the left and right panel of Fig. 4, both superposed on the POSS-2 plate. The left panel shows the full resolution image, while in the right panel lower resolution contours are displayed. Figure 5 shows the same region overlaid on the X-ray ASCA image. Our images confirm that RXCJ 1314.4–2515 has a complex radio morphology, with the presence of three different regions of extended emission on the cluster scale.

Two parallel features are easily visible in Figs. A.2, 4 and 5. They are separated by ∼6′ and extend in the SE-NW direction for approximately 4′ (i.e. ∼910 kpc at the cluster redshift). The

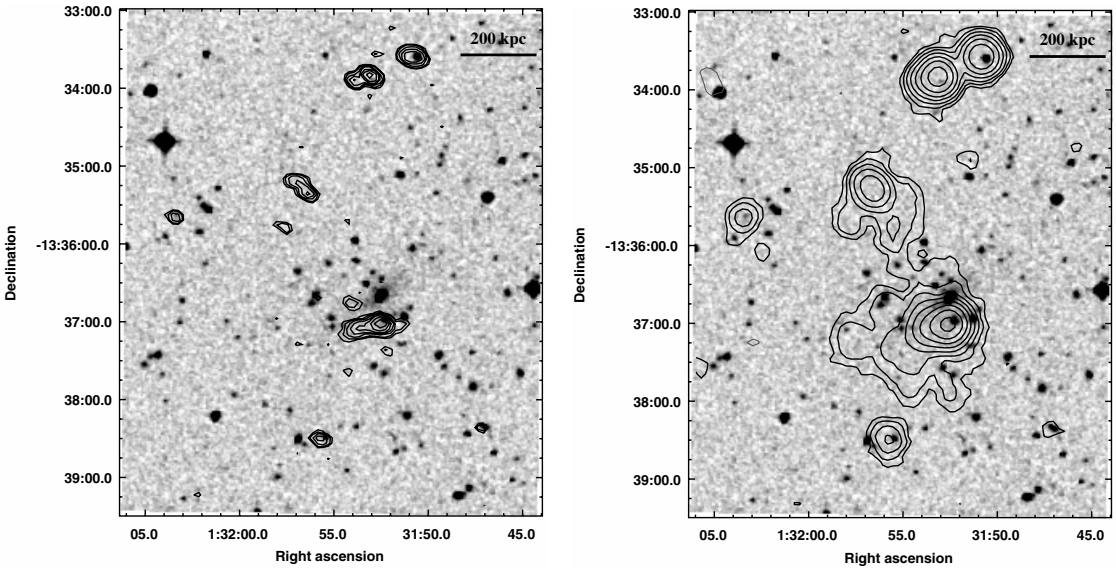

Fig. 2. *Left* – GMRT 610 MHz radio contours for the A 209 cluster superposed on the POSS–2 optical plate. The 1σ level in the image is 60 μJy b^{-1}. Contours are $0.3 \times (\pm 1, 2, 4, 8, 16...)$ mJy b^{-1}. The HPWB is $8.0'' \times 5.0''$, PA 64°. *Right* – Natural weighted image of the same sky region at the resolution of $18.0'' \times 17.0''$, PA 0°. The rms (1σ) in the image is 60 μJy b^{-1}, contours are $0.18 \times (\pm 1, 2, 4, 8, 16...)$ mJy b^{-1}.

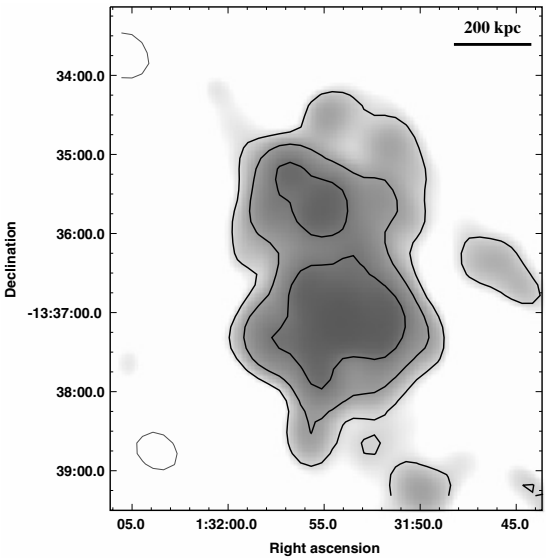

Fig. 3. Radio contours over grey scale of the A 209 cluster radio halo after subtraction of the individual radio sources (see left panel of Fig. 2 and Sect. 4.1.1 in the text). The resolution of this image is $32.0'' \times 30.0''$, PA 30°. The rms (1σ) in the image is 0.15 mJy b^{-1}, contours are $0.35 \times (\pm 1, 2, 4, 8, 16...)$ mJy b^{-1}.

remarkable superposition of the low resolution radio image with the ASCA image in Fig. 5 clearly shows that these two sources are located at the border of the detected X-ray emission.

The overall morphology of these two features, coupled with their location with respect to the intracluster gas, suggest that they are radio relics, as also discussed in Feretti et al. (2005), who ruled out any association with individual galaxies. In the following we will refer to the eastern and the western relics as E-R and W-R respectively, as also labelled in Fig. 4. The morphology and flux density ratio of the two relics are consistent with the 1.4 GHz data in Feretti et al. (2005). Their flux densities at 610 MHz are $S_{610\ \mathrm{MHz}} = 64.8 \pm 3.2$ mJy and $S_{610\ \mathrm{MHz}} = 28.0 \pm 1.4$ mJy for W-R and E-R respectively. The value given for E-R does not include the southernmost pointlike source A (Fig. 4). In order to derive the total spectral index of W-R and E-R between 1.4 GHz and 610 MHz we included also the contribution of source A to the flux density of E-R, for a consistent comparison with Feretti et al. (2005), and obtained 32.8 mJy. Our flux density measurements lead to the same value for the spectral index in both features. In particular, $\alpha^{1.4\ \mathrm{GHz}}_{610\ \mathrm{MHz}}$(W–R) = 1.40 ± 0.09 and $\alpha^{1.4\ \mathrm{GHz}}_{610\ \mathrm{MHz}}$(E–R) = 1.41 ± 0.09.

Figures 4 (right panel) and 5 show that extended emission is present in the region between W-R and E-R, consistent with the 1.4 GHz VLA images in Feretti et al. (2005), who classified this feature as a radio halo. This source is referred to as RH in the right panel of Fig. 4. It is spatially coincident with the bulk of the optical galaxies (see Valtchanov et al. 2002) and its largest angular size is ∼2′, corresponding to 460 kpc, i.e. it is not a giant radio halo. The radio halo seems to blend with the emission of the western relic W-R, however it is difficult to say whether this is a true feature, since projection effects are likely to play a role. Given the different polarisation properties of radio halos and relics, polarisation information would be necessary to investigate this issue. We measured a flux density of $S_{610\ \mathrm{MHz}} = 10.3 \pm 0.3$ mJy for the radio halo. No spectral index estimate between 610 MHz and 1.4 GHz can be derived, due to the lack of a flux density value at 1.4 GHz (Feretti et al. 2005).

4.1.4. RXCJ 2003.5–2323

RXCJ 2003.5–2323 is the most distant cluster in our sample, with $z = 0.3171$ ($1'' = 4.626$ kpc). Little information is available in the literature. The ROSAT All Sky Survey (RASS) image shows that the X-ray emission is elongated along the NW-SE direction, which might suggest a disturbed dynamical status for RXCJ 2003.5–2323.

Our GMRT 610 MHz observations show that it is the most striking cluster among those observed thus far. It hosts a *giant* radio halo, one of the largest known up to date. Its largest angular size is ∼5′, corresponding to ∼1.4 Mpc. Hints of the presence of this very extended radio halo were clear already from inspection of the NRAO VLA Sky Survey (NVSS).

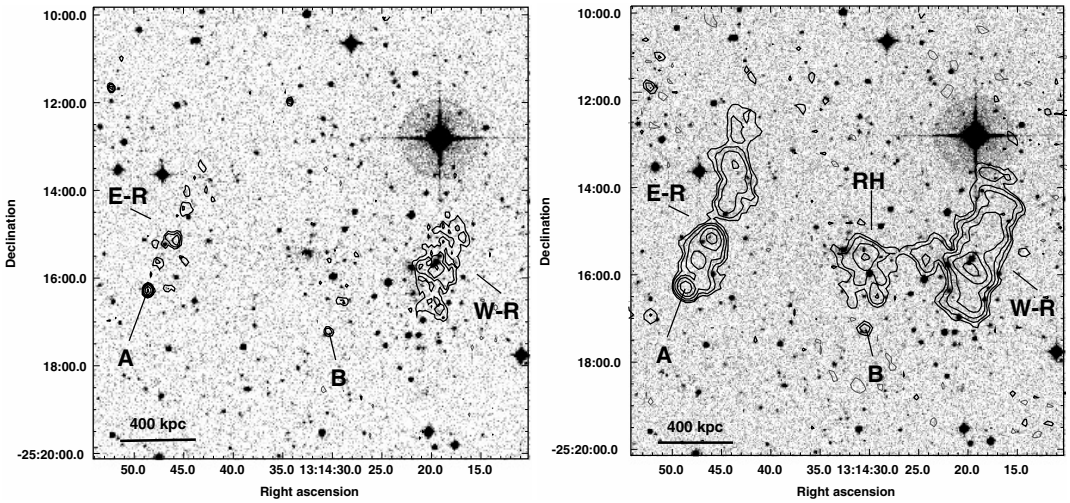

Fig. 4. *Left* – GMRT 610 MHz radio contours for the cluster RXCJ 1314.4–2515 superposed on the POSS-2 optical plate. The 1σ level in the image is 60 μJy b^{-1}. Contours are $0.18 \times (\pm 1, 2, 4, 8, 16...)$ mJy b^{-1}. The HPWB is $8.0'' \times 5.0''$, PA 15°. The western and the eastern relics are labelled as E-R and W-R respectively, and the individual point sources in the relics/halo region are indicated as A and B. *Right* – GMRT 610 MHz radio contours for the cluster RXCJ 1314.4–2515 superposed on the POSS-2 optical plate. The 1σ level in the image is 60 μJy b^{-1}. Contours are $0.2 \times (\pm 1, 2, 4, 8, 16...)$ mJy b^{-1}. The HPWB is $20.0'' \times 15.0''$, PA 39° The western and the eastern relics are labelled as E-R and W-R respectively, RH indicates the radio halo, and the individual point sources in the relics/halo region are indicated as A and B.

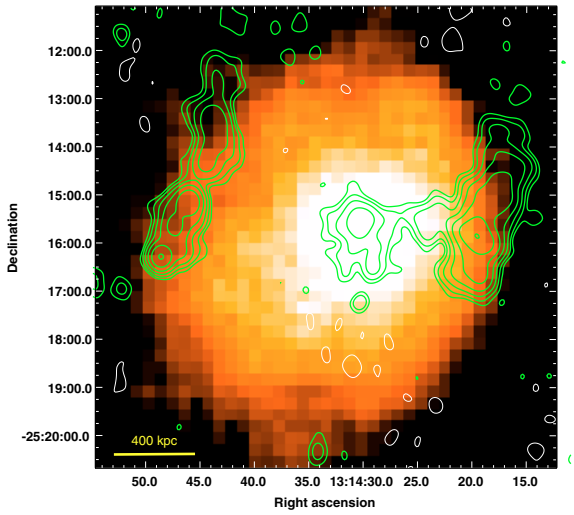

Fig. 5. GMRT 610 MHz radio contours for the cluster RXCJ 1314.4–2515 superposed on the X-ray archive ASCA image (colour). The 1σ level in the image is 60 μJy b^{-1}. Contours are $0.18\times(\pm 1, 2, 4, 8, 16...)$ mJy b^{-1}. The HPWB is $25.0'' \times 22.0''$, PA 15°.

The cluster radio emission within the cluster virial radius is given in Fig. A.3. The central part of the cluster is shown in Fig. 6. The left panel shows a full resolution image superposed to the POSS-2 optical image, to highlight the individual sources (labelled from A to H). The sources with a clear optical counterpart (B to H) were subtracted from the u-v data when producing the image shown in the right panel of Fig. 6, which we convolved with a larger beam in order to highlight the low surface brightness emission. We did not subtract A, since no optical counterpart is visible on the POSS-2, therefore we consider this feature as a peak in the radio halo emission. One of the most striking features of this giant radio halo is its complex morphology: clumps and filaments are visible on angular scales of the order of $\sim 1'$ (clumps) and ~ 2–$3'$ (filaments), as clear from Figs. A.3 and 6 (right panel). Unfortunately no deep X-ray images are available for this cluster, therefore a combined radio and X-ray analysis cannot be carried out. The only information we can derive from the RASS image of the cluster is that the whole radio emission from the halo is embedded within the X-ray emission, as shown in Fig. 7.

The total flux density of the radio halo (after subtraction of the point sources) is $S_{610\ \mathrm{MHz}} = 96.9 \pm 5.0$ mJy, corresponding to $\log P_{610\ \mathrm{MHz}}$ (W/Hz) = 25.49.

4.2. Candidate extended emission in Abell 3444

Abell 3444 (RXCJ 1023.8−2715, $z = 0.2542$, $1'' = 3.924$ kpc) was indicated as possible cooling core cluster by Lémonon (1999) and Matsumoto (2001) on the basis of the analysis of ASCA data, though at limited significance. The X-ray ASCA image shows that the inner part of the cluster is elongated along the SE-NW direction.

No radio information is reported in the literature. Unfortunately, due to calibration problems, we could use only the USB of our dataset to image this cluster. Our GMRT 610 MHz image of the radio emission within the cluster virial radius is reported in Fig. A.4, and shows that the radio emission is dominated by a chain of individual sources, all with optical counterpart from the POSS-2. The alignment of the chain of radio galaxies is in agreement with the inner elongation of the archive ASCA X-ray image.

A radio-optical overlay of the central part of the field is given in Fig. 8 (Left). The extended radio galaxy at the north-western end of the chain is associated with the dominant cluster galaxy (right panel in Fig. 8). Its morphology is complex. Bent emission in the shape of a wide angle tail is clear in the inner part of the source, surrounded by extended emission. At least a couple of very faint objects are visible in the same region of the extended radio emission, so it is unclear if we are dealing with extended emission associated with the dominant cluster galaxy, or if this feature is the result of a blend of individual sources. Under the assumption that all the emission detected within the 3σ contour (left panel of Fig. 8) is associated with the dominant cluster galaxy, we measured a flux density $S_{610\ \mathrm{MHz}} = 16.5 \pm 0.8$ mJy, which corresponds to $\log P_{610\ \mathrm{MHz}}$(W/Hz) = 24.51. The largest

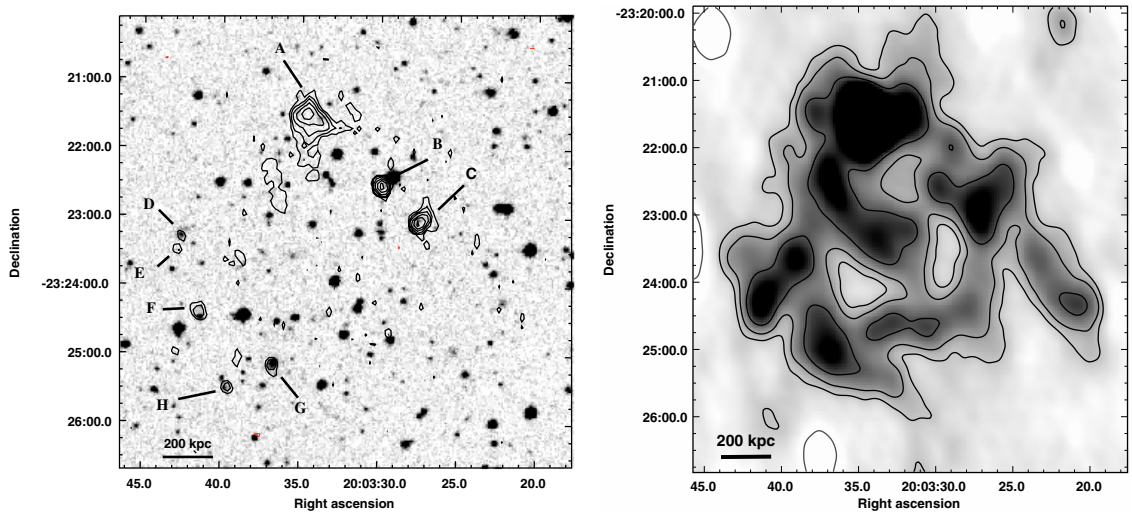

Fig. 6. *Left* – Full resolution GMRT 610 MHz contours of the central region of RXCJ 2003.5–2323, superposed to the POSS-2 optical image. The resolution of the radio image is 6.9″ × 5.0″, PA −0.3°, the 1σ level is 40 μJy b^{-1}. Contours are 0.12 × (±1, 2, 4, 8...) mJy b^{-1}. Individual sources are labelled from A to H. *Right* – GMRT 610 MHz gray scale and radio contours of the giant radio halo in RXCJ 2003.5–2323 after subtraction of the individual sources (from B to H in the left panel). The HPWB is 32.0″ × 23.0″, PA 15°. Contours are 0.3 × (±1, 2, 4, 8...) mJy b^{-1}. The 1σ level in the image is 100 μJy b^{-1}.

Table 3. Parameters of the extended cluster radio sources.

Cluster	Source Type	$S_{610\ \mathrm{MHz}}$ mJy	log $P_{610\ \mathrm{MHz}}$ W Hz^{-1}	LAS arcmin	LLS kpc	L_1/L_2
A 209	Giant Halo	24.0 ± 3.6	24.46	~4	~810	~2
A 521	Relic	41.9 ± 2.1	24.91	~4	~930	~4.5
RXCJ 1314.4–2515	Western Relic	64.8 ± 3.2	25.03	~4	~910	~3
	Eastern Relic	28.0 ± 1.4	24.67	~4	~910	~4.3
	Halo	10.3 ± 0.3	24.22	~2	~460	~1.5
RXCJ 2003.5–2323	Giant Halo	96.9 ± 5.0	25.49	~5	~1400	~1.3
A 3444	Central Galaxy	16.5 ± 0.8	24.51	~0.7	~165	~1.4
	surrounding Halo	10.0 ± 0.8	24.29	~1.5	~350	~1.4

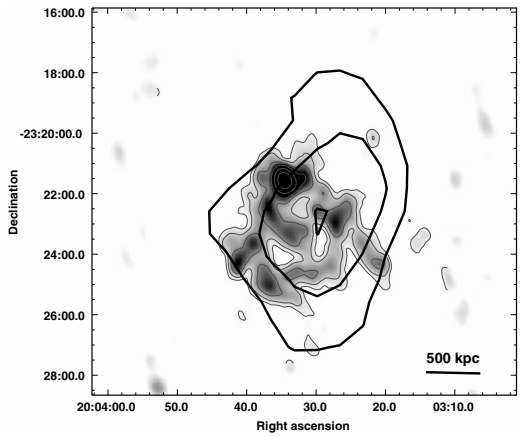

Fig. 7. ROSAT All Sky Survey contours (black) of RXCJ 2003.5–2323 overlaid on the 610 MHz gray scale and contours (gray) of the radio halo. The X-ray contours levels are logarithmically spaced by a factor of $\sqrt{2}$. The radio image is the same as right panel of Fig. 6.

angular size of the radio source is ~40″, hence the linear size is ~165 kpc.

Both panels of Fig. 8 suggest that emission on a larger scale may be present around the central radio source. Indeed we measured a flux density of $S_{610\ \mathrm{MHz}}$ = 10.0 ± 0.8 mJy on an angular scale of ~1.5′, i.e. ~350 kpc.

This situation is reminiscent of the class of core-halo sources, where extended emission surrounds a radio component obviously associated with a galaxy. Core-halo sources are usually located in cooling core clusters. Some well-known examples are 3C 317 (Zhao et al. 1993), 3C84 (Böhringer et al. 1993), PKS 0745–191 (Baum & O'Dea 1991).

4.3. Galaxy clusters without extended emission

For the remaining six clusters our 610 MHz GMRT observations did not show any indication of possible extended emission at the noise level of the final images.

4.3.1. S 780

S 780 (RXCJ 1459.4–1811, z = 0.2357, 1″ = 3.952 kpc) is the most X-ray luminous and most massive cluster among those presented in this paper. No information is available in the literature. Inspection of the ROSAT archive indicates that the X-ray emission is elongated in the E-W direction.

Figure A.5 reports the 610 MHz contours of the S 780 field within the virial radius. The radio emission from S 780 is typical of a very active cluster, with a number of cluster-type radio galaxies. Beyond the dominant central radio source, one

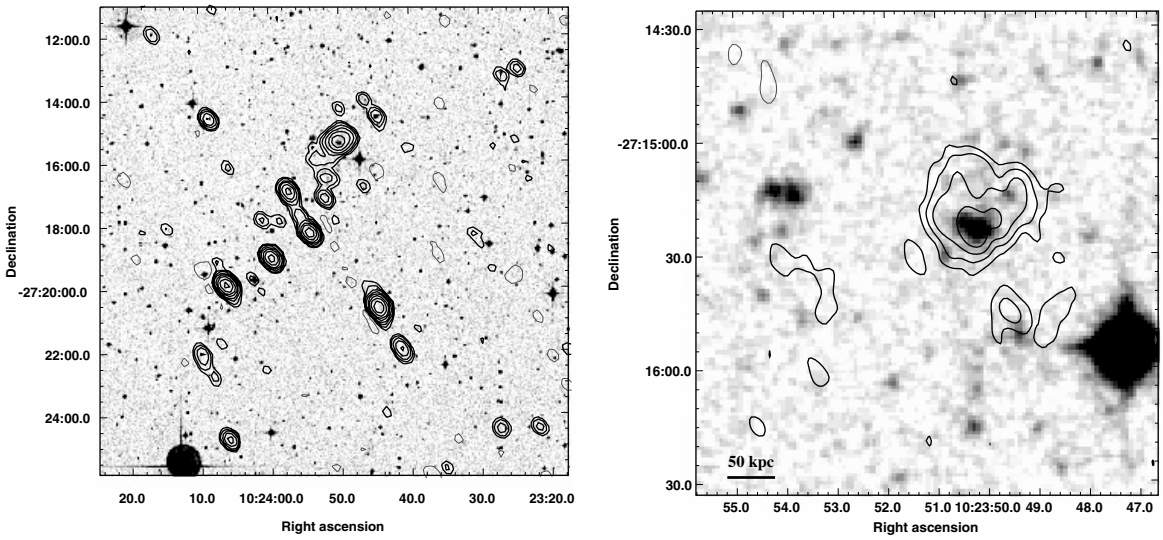

Fig. 8. *Left* – GMRT 610 MHz radio contours for the cluster A 3444 superposed on the POSS-2 optical plate. The 1σ level in the image is $\sim$50 μJy b^{-1}. Contours are 0.15 $\times$ ($\pm$1, 2, 4, 8, 16...) mJy b^{-1} (3σ). The HPWB is 23.2″ $\times$ 16.1″, PA 37.6°. *Right* – High resolution zoom on the central cluster galaxy. The HPBW is 7.6″ $\times$ 4.9″, PA 19°. Contours are given starting from the 3σ level: 0.20 $\times$ ($\pm$1, 2, 4, 8...).

head-tail radio galaxy is clearly visible close to the cluster centre, one wide-angle tail is located at $\sim$6′ from the cluster centre (well within the virial radius) and one FRII radio galaxy (Fanaroff & Riley 1974) with distorted jets is located at $\sim$8′ from the cluster centre (in the S-E direction). A few more radio sources in the cluster field are optically identified. A visual inspection of the optical counterparts of all these radio sources suggests they have similar optical magnitudes.

Radio-optical overlays are given in Fig. 9. The left panel shows the central part of the cluster superposed on the POSS-2 optical frame, and the right panel is a high resolution zoom of the central cluster galaxy. The radio galaxy shows a compact component coincident with the nucleus of the associated galaxy, extended emission in the eastern direction and a filament aligned South-East. The total angular size is $\sim$50″, corresponding to a largest linear size LLS $\sim$200 kpc. The flux density is $S_{610\ \mathrm{MHz}} = 135.9 \pm 6.8$ mJy, i.e. $\log P_{610\ \mathrm{MHz}}(\mathrm{W/Hz}) = 25.32$. Sources A and B highlighted in the right panel of Fig. 9 were not included in the flux density measurement. The flux density of the filament just South of the central radio source is $S_{610\ \mathrm{MHz}} = 3.1 \pm 0.2$ mJy. No indication of residual flux density is present in the cluster centre.

4.3.2. Abell 2697

Very little information is available in the literature for A 2697 (RXCJ 0003.1–0605, $z = 0.2320$, 1″ = 3.698 kpc). Archive X-ray ROSAT and ASCA images show that the hot intracluster gas has a fairly regular distribution.

For this cluster only one portion of the band (USB) was available. We imaged the cluster in a range of resolutions, reaching a 1σ noise level of $\sim$80 μJy b^{-1} in each image. The radio field is dominated by a head-tail galaxy. Radio contours are reported in Fig. A.6 in the Appendix.

No cluster-type extended feature is visible at the sensitivity level of the images, and no significant flux density from positive residuals were found by integrating over a wide region of the cluster centre.

4.3.3. Abell 141

The X-ray emission of A 141 (RXCJ 0105.5–2439, $z = 0.2300$, 1″ = 3.674 kpc) is bimodal. The archive X-ray ROSAT images show that the North-South elongation of the ASCA image is the result of two components, the northern one being the brightest and largest. The same orientation was found also in the distribution of the cluster galaxies by Dahle et al. (2002), who concluded that the overall optical analysis is suggestive of recent merger activity. Those authors reported also evidence of weak lensing.

High resolution radio imaging aimed at the detection of cluster radio galaxies was carried out with the VLA-A at 1.4 GHz by Rizza et al. (2003).

For this cluster only one portion of the observing band (USB) was available. Our GMRT observations of A 141 revealed neither the presence of diffuse emission at the level of $\sim$100 μJy b^{-1}, nor unusually high residuals. Radio contours are reported in Fig. A.7 in the Appendix.

4.3.4. Abell 3088

Very little information is available in the literature for A3088 (RXCJ 0307.0–2840, $z = 0.2537$, 1″ = 3.952 kpc). It is a richness 2 galaxy cluster with a very regular and symmetric X-ray morphology. On the basis of XMM-Newton observations, Zhang et al. (2006) reported a gas temperature $kT = 6.4 \pm 0.3$ keV and classified it as a "single dynamical state" cluster with a cooling core (Finoguenov et al. 2005).

Our GMRT 610 MHz observations show that the field has only a few radio sources, with a lack of positive residual flux density in the central cluster region and no hints of diffuse emission from the cluster at the detection level of our images, i.e. $1\sigma \sim 65$ μJy b^{-1}. Contours of the radio emission within the cluster virial radius are shown in Fig. A.8.

4.3.5. Abell 2537

Little information is available in the literature for A 2537 (RXCJ 2308.2–0211, $z = 0.2966$, 1″ = 4.419 kpc). Archive HST observations show the presence of several red and blue arcs, and Dahle et al. (2002) report evidence of weak lensing.

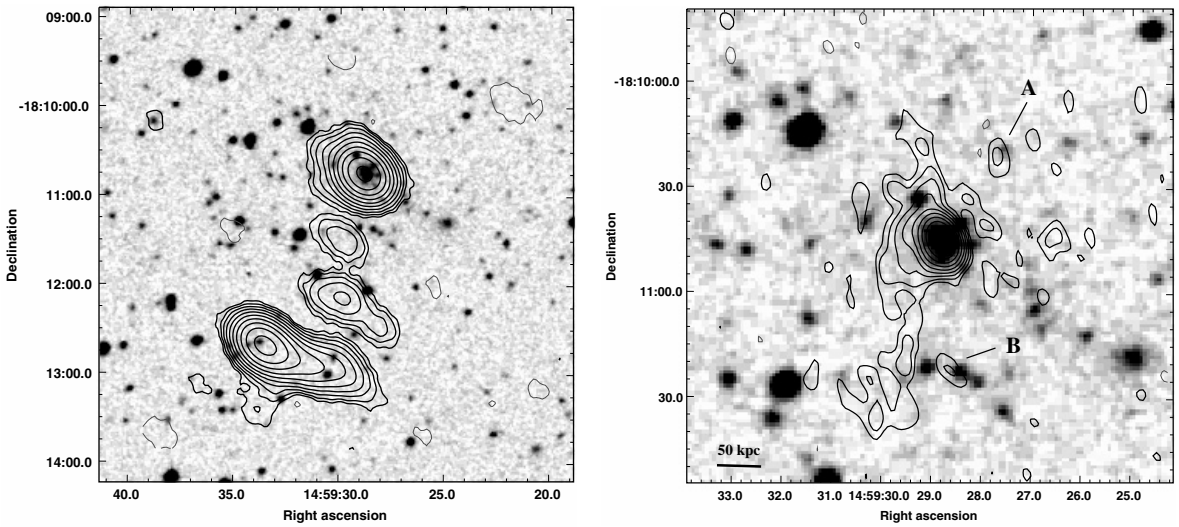

Fig. 9. *Left* – GMRT 610 MHz radio contours for the cluster S 0780 superposed on the POSS-2 optical plate. The 1σ level in the image is 65 μJy b^{-1}. Contours are $0.20 \times (\pm 1, 2, 4, 8, 16...)$ mJy b^{-1}. The HPWB is $20.9'' \times 15.9''$, PA 45.9°. *Right* – High resolution zoom on the central cluster galaxy. The HPWB is $7.5'' \times 5.0''$, PA 25°. Contours are $0.19 \times (\pm 1, 2, 4, 8, 16...)$ mJy b^{-1} (first contous is 3σ).

The cluster was observed in the X-ray band by XMM-Newton and was classified as "single dynamical state", with gas temperature $kT = 7.9 \pm 0.7$ keV (Zhang et al. 2006). A secondary X-ray peak is present at $\sim 7'$ from the cluster gas concentration.

For this cluster only the USB provided useful data. The 610 MHz radio emission from the cluster, shown in Fig. A.9 is dominated by a tailed radio galaxy located at the cluster centre. Very few other radio sources are detected above the 5σ level of the image. No hint of extended emission is present in the field at the level of ~ 60 μJy b^{-1} (1σ), and no high positive flux density residuals were detected over the central cluster region.

4.3.6. Abell 2631

Little information is available in the literature for the rich cluster A 2631 (RXCJ 2337.6+0016, $R = 3$, $z = 0.2779$, $1'' = 4.221$ kpc). Archive ROSAT X-ray images are available for A 2631, which show a complex morpholgy. Based on XMM-Newton observations Zhang et al. (2006) classified it as "offset centre", with varying isophote centroids on different angular scales, and reported a gas temperature $kT = 9.6 \pm 0.3$ keV. Finoguenov et al. (2005) interpret the XMM properties of this cluster in terms of a late stage of a core disruption. The cluster was observed with the VLA-A at 1.4 GHz (Rizza et al. 2003).

Our GMRT observations of this cluster were spread over two days, however on both days only one portion of the band (USB) was available. The 610 MHz radio emission of A 2631 within the virial radius is shown in Fig. A.10. It is dominated by a central tailed radio galaxy and all the remaining sources above the 5σ level are located South of the cluster centre. No signs of extended emission are present in the field at the rms level of ~ 50 μJy b^{-1} (1σ), and no positive residuals were found by integrating over the central region of the cluster.

5. Discussion and conclusions

Our 610 MHz GMRT radio halo survey has been designed in order to statistically investigate the connection between cluster merger phenomena and the presence of cluster-scale radio emission. In particular, our main goal is to derive the fraction of massive clusters (i.e. $M \geq 10^{15}$ $M_{\odot}$) with giant radio halos in the redshift range $0.2 < z < 0.4$, in order to constrain the expectations made by CBS04 and CB05 in the framework of the particle re-acceleration model. The total cluster sample consists of two sub-samples of massive clusters extracted from the REFLEX and extended BCS catalogues, and includes a total of 50 clusters.

The cluster sample presented here (see Table 1) includes 27 REFLEX clusters, eleven of which were observed in a first run of GMRT observations carried out in January 2005. If we consider the literature data, information is now available for 15 of the 27 objects. The most relevant results we obtained, as well as the status of the observations for the remaining clusters in the sample are summarized below.

(a) Two new giant radio halos were found, i.e. A 209 (also reported in Giovannini et al. 2006, while this paper was in preparation), and RXCJ 2003.5–2323, discovered with the present 610 MHz GMRT observations.
(b) A radio halo (LLS $\sim$ 460 kpc) was found in RXCJ 1314.4–2515.
(c) Two relics were found in the cluster RXCJ 1314.4–2515, and one in A 521 (Giacintucci et al. 2006). These three relics are impressive structures. Their largest linear size is of the order of the Mpc, which suggests that particle acceleration, most likely related to the hierarchical formation of clusters and accretion processes, might be required to account for their formation (e.g. Ensslin & Brüggen 2002). The relic in A 521 has already been studied in detail. Here we just wish to mention that RXCJ 1314.4–2515 is the third galaxy cluster known to date hosting two relics, after A 3667 (Roettiger et al. 1999; Johnston-Hollitt et al. 2002) and A 3376 (Bagchi et al. 2006). Furthermore, it is unique in hosting two relic sources and one radio halo, and hence a challenge for our understanding of the connection between radio halos, relics and the physics of cluster mergers.
(d) Extended emission on smaller scale (of the order of $\sim$350 kpc) was detected around the dominant galaxy in A 3444, whose radio morphology and monocromatic power are similar to those of core-halo radio galaxies found at the centre of cooling core clusters.

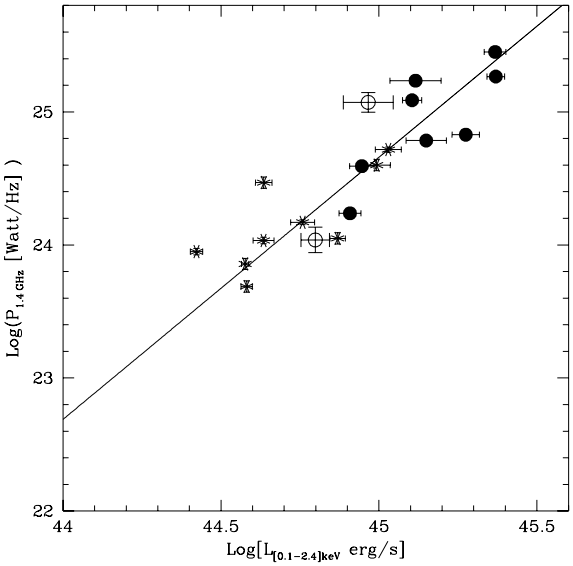

Fig. 10. Log L_X–Log $P_{1.4\ GHz}$ plot for the clusters with detected giant radio halos. Stars represent the literature clusters at $z < 0.2$ and filled circles the literature clusters at $z > 0.2$. Open circles show the location of A 209 (*lower left*) and RXCJ 2003.5–2323 (*upper right*).

(e) Three clusters in the sample host well-known giant radio halos, i.e. A2744 (Govoni et al. 2001), A1300 (Reid et al. 1999) and A2163 (Herbig & Birkinshaw 1994; Feretti et al. 2001).
(f) No extended emission of any kind was detected at the level of 50–100 μJy b^{-1} in six of the 11 clusters observed by us and presented here.
(g) The cluster RXCJ 0437.1+0043 is known not to host extended emission, based on low resolution 1.4 GHz VLA observations (Feretti et al. 2005).
(h) Five clusters were observed by us in October 2005, two more will be observed in August 2006, and they will be presented in a future paper (see Sect. 3).
(i) The remaining 5 clusters are being observed by other authors (GMRT Cluster Key Project, P.I. Kulkarni) and no literature information is available thus far.

In Fig. 10 we show the location of the giant radio halos in A 209 and RXCJ 2003.5–2323 in the log L_X–log ($P_{1.4\ GHz}$) plane, where all the previously known clusters with giant radio halos are also reported (see CBS06 and references therein for the literature data). The radio power at 1.4 GHz for these two clusters was obtained scaling the measured flux density at 610 MHz with a spectral index $\alpha_{610\ MHz}^{1.4\ GHz} = 1.2 \pm 0.2$ (the uncertainty assumed here dominates over the 610 MHz flux density error). Clusters at $z < 0.2$ and those at $z > 0.2$ are shown with different symbols. Despite some overlap, the most powerful radio halos are hosted in the most X-ray luminous clusters, which are also the most distant. The location of A 209 and RXCJ 2003.5–2323 on the plot is in good agreement with the distribution of all giant radio halos known in the literature.

An important piece of information would be the knowledge of the merging stage of the clusters in the sample, since cluster merger is a major ingredient in the re-acceleration model. The literature information on the clusters presented here is not homogenous, and it is not possible to make conclusive statements on the connection between merging/non-merging signatures and the presence/absence of radio halos. A 209 is known to be undergoing merging events, but no information is available for RXCJ 2003.5–2323, except for the elongated X-ray emission imaged by ROSAT. The three radio halo clusters known from the literature are all reported to be dynamically active (see for instance Zhang et al. 2006; and Finoguenov et al. 2005). Signature of cluster merger is present in the optical and X-ray bands for A 521 (Giacintucci et al. 2006; and references therein) and RXCJ 1314.4–2515, which host extended radio emission in the form of radio halo and relics. Elongated or more complex X-ray isophotes are visible in S 780, A 141, A 2631 and in RXCJ 0437.1+0043, which lack cluster scale radio emission. The remaining two clusters without extended emission are considered "relaxed" on the basis of the X-ray emission

To summarize, the optical and X-ray information for the sample of clusters presented here is not inconsistent with the findings that clusters with radio halos are characterised by signatures of merging processes. On the other hand, clusters without extended radio emission may or may not show dynamical activity at some level. This crucial issue will be further investigated in future works.

In the framework of the canonical particle re-acceleration model giant radio halos are believed to be essentially an on/off phenomenon, triggered by dissipation via collisionless damping of turbulence injected during cluster mergers.

The physics of collisionless turbulence and of particle acceleration is still poorly understood and many hidden ingredients could be of relevance in computing the efficiency of the particle acceleration processes in the ICM. On the other hand, from simple energetic arguments, it is clear that the possibility to develop a giant radio halo is related to the efficiency of turbulence injection and to the possibility to generate large enough (≥Mpc sized) turbulent cluster regions. In this respect, the calculations in CBS04, CB05 and more recently in CBS06 show that major cluster mergers (i.e. with mass ratio of the order ≤5:1) between massive clusters ($M \geq 10^{15}\ M_\odot$) may provide the necessary ingredients to develop giant radio halos. During these mergers a fraction of up to ∼10% of the cluster thermal energy is believed to be injected in a ∼Mpc^3 region. However, from a theoretical point of view, it is hard to predict if a particular merging clusters may host a giant radio halo, since this depends on a number of parameters which cannot be easily estimated. For instance, in order to have enough time for the turbulence injected on large scales to cascade down to collisionless scales, it is necessary that seed relativistic particles (to be reaccelerated) are present in the turbulent ICM, and that the magnetic field in the ICM is strong enough to allow ∼GeV electrons to emit synchrotron radiation at the observed frequency.

The statistical approach developed in CBS04, CB05 and CBS06 allows a more reliable estimate of the fraction of clusters hosting a giant radio halo. Without going into the calculation details, the most relevant result in the light of those papers is that the fraction of galaxy clusters with mass ∼2–3.5 × $10^{15}\ M_\odot$ and redshift $z = 0.2 \div 0.4$ expected to host a giant radio halo is in the range ∼10–35%. In addition, CBS06 showed that the cluster magnetic field plays an important role, and that this fraction depends the scaling law between the magnetic field and cluster mass.

Radio information is now available for 15 of the 27 clusters considered in this paper, and 5 of them possess a giant radio halo. However, at this stage of our work the statistics are still poor, and no firm comparison with theoretical expectations can be reached. For this reason our analysis, in the light of the predictions made in CB05 and CBS06, will be carried out as soon as the information on the whole selected sample (REFLEX and BCS) is completed (Venturi et al. in prep.; Cassano et al. in prep.).

Acknowledgements. We thank the staff of the GMRT for their help during the observations. GMRT is run by the National Centre for Radio Astrophysics of the Tata Institute of Fundamental Research. T.V. and S.G. acknowledge partial support from the Italian Ministry of Foreign Affairs. G.B., R.C. and G.S. acknowledge partial support from MIUR grants PRIN2004 and PRIN2005.

Appendix A: Radio images

In this appendix we report the 610 MHz radio contours of all the observed clusters in the present project. The images cover the region within the cluster virial radius. The resolution is $15.0'' \times 12.0''$ in all the images, except for A209, RXCJ 1314.4–2515 and RXCJ 2003.5–2323 (see figure caption).

References

Bacchi, M., Feretti, L., Giovannini, G., et al. 2003, A&A, 400, 465
Bagchi, J., Durret, F., Lima Neto, G. B., et al. 2006, Science, 314, 791
Baum, S. A., & O'Dea, C. P. 1991, MNRAS, 250, 737
Blasi, P. 2004, JKAS, 37, 483
Böhringer, H., Voges, W., Fabian, A. C., et al. 1993, MNRAS, 264, 25
Böhringer, H., Schuecker, P., Guzzo, L., et al. 2004, A&A, 425, 367
Brunetti, G. 2003, in Matter and Energy in Clusters of Galaxies, ed. S. Bowyer, & C.-Y. Hwang, San Francisco: Astron. Soc. Pac., ASP Conf. Ser., 301, 349
Brunetti, G. 2004, JKAS, 37, 493
Brunetti, G., Setti, G., Feretti, L., et al. 2001, MNRAS, 320, 365
Brunetti, G., Blasi, P., Cassano, R., et al. 2004, MNRAS, 350, 1174
Buote, D. A. 2001, ApJ, 553, 15
Cassano, R., & Brunetti, G. 2005, MNRAS, 357, 1313 (CB05)
Cassano, R., Brunetti, G., & Setti, G. 2004, JKAS, 37, 589 (CBS04)
Cassano, R., Brunetti, G., & Setti G. 2006, MNRAS, 369, 1577 (CBS06)
Dahle, H., Kaiser, N., Irgens, R. J., et al. ApJS, 139, 313
Ebeling, H., Edge, A. C., Böhringer, H., et al. 1998, MNRAS, 301, 881
Ebeling, H., Edge, A. C., Allen, S. W., et al. 2000, MNRAS, 318, 333
Ensslin, T. A., 2004, JKAS, 37, 439
Ensslin, T. A., & Brüggen, M. 2002, MNRAS, 331, 1011
Fanaroff, B. L., & Riley, J. M. 1974, MNRAS, 167, 31
Feretti, L. 2003, XXI Symposium on Relativistic Astrophysics, ed. R. Bandiera, R. Maiolino, & F. Mannucci (World Scientific Publishing), 209
Feretti, L., Fusco-Femiano, R., Giovannini, G., et al. 2001, A&A, 373, 106
Feretti, L., Gioia, I. M., & Giovannini, G. 2002, Merging Processes in Galaxy Clusters, ASSL, 272
Feretti, L., Schuecker, P., Böhringer, H., et al. 2005 A&A, 444, 157
Finoguenov, A., Böhringer, H., & Zhang, Y.-Y. 2005 A&A, 442, 827
Fujita, Y., Tazikawa, M., & Sarazin, C. L. 2003, ApJ, 584, 190
Giacintucci, S., Venturi, T., Bardelli, S., et al. 2006, New Astron., 11, 437
Giovannini, G., & Feretti, L. 2002, in Merging Processes in Galaxy Clusters, ed. L. Feretti, I. M. Gioia, & G. Giovannini, ASSL, 272, 197
Giovannini, G., & Feretti, L. 2004, J. Korean Astr. Soc., 37, 323
Giovannini, G., Tordi, M., & Feretti, L. 1999, New Astron., 4, 141
Giovannini, G., Feretti, L., Govoni, F., et al. 2006, in Origin and Evolution of Cosmic Magnetism, Astron. Nachr., 327, 563
Govoni, F., Feretti, L., Giovannini, G., et al. 2001, A&A 376, 803
Haines, C. P., Mercurio, A., Merluzzi, P., et al. 2004, A&A, 425 783
Herbig, T., & Birkinshaw, M., 1994, BAAS, 26, 1403
Hwang, C.-Y. 2004, JKAS, 37, 461
Johnston-Hollitt, M., Clay, R. W., Ekers, R.D, et al. 2002, in The Universe at Low Radio Frequencies, ed. A. P. Rao, G. Swarup, & Gopal-Krishna, IAU Symp., 199, 157
Kempner, J. C., & Sarazin, C. L. 2001, ApJ, 548, 639
Lémonon, L., 1999, Ph.D. Thesis Université de Paris XI
Matsumoto, H., Pierre, M., Tsuru, T. G., et al. 2001, A&A, 374, 28
Mercurio, A., Girardi, M., Boschin, W., et al. 2003, A&A, 397, 431
Mercurio, A., 2004a, Ph.D. Thesis, University of Trieste, [arXiv:astro-ph/0412077]
Mercurio A., Busarello, G., & Merluzzi, P. 2004b, A&A, 424, 79
Petrosian, V. 2001, ApJ, 557, 560
Reid, A. D., Hunstead, R. W., Lemonon, L., et al. 1999, MNRAS, 302, 571
Reiprich, T. H., & Böhringer, H. 2002 ApJ, 567, 716
Rizza, E., Burns, J.O, Ledlow, M.J, et al. 1998, MNRAS, 301, 328
Rizza, E., Morrison, G. E., Owen, F. N., et al. 2003, ApJ, 126, 119
Roettiger, K., Burns, J. O., & Stone, J. M. 1999, ApJ, 518, 603
Sarazin, C. L., in Merging Processes in Galaxy Clusters, ed. L. Feretti, I. Gioia, & G. Giovannini, ApS&S Library (Dordrecht, Kluwer), 272, 1
Tribble, P. C. 1993, MNRAS, 263, 31
Valtchanov, I., Murphy, T., Pierre, M., et al. 2002, A&A, 392, 795
Zhang, Y. Y., Böhringer, H., Finoguenov, A., et al. 2006, A&A, 456, 55
Zhao, J. H., Sumi, D. M., & Burns, J. O. 1993, ApJ, 461, 51

Online Material

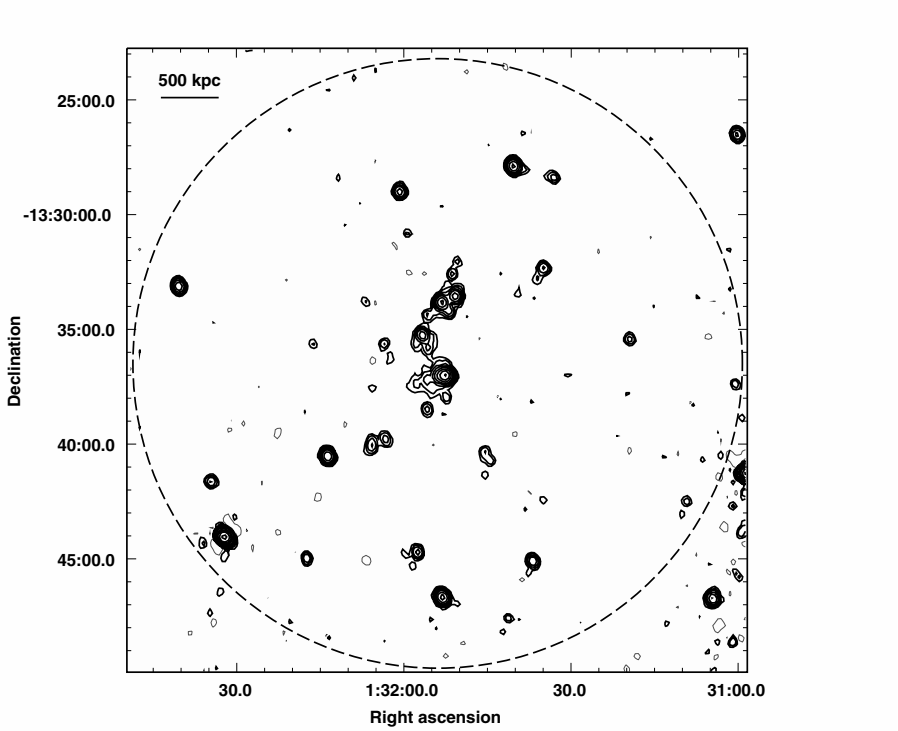

Fig. A.1. GMRT 610 MHz radio contours for the cluster A 209. The 1σ level in the image is 50 μJy b^{-1}. Contours are 0.20 × (±1, 2, 4, 8, 16...) mJy b^{-1}. The HPWB is 21.0″ × 18.0″, PA 13°. The radius of the dashed circle is the virial radius, corresponding to 13.28′ for this cluster.

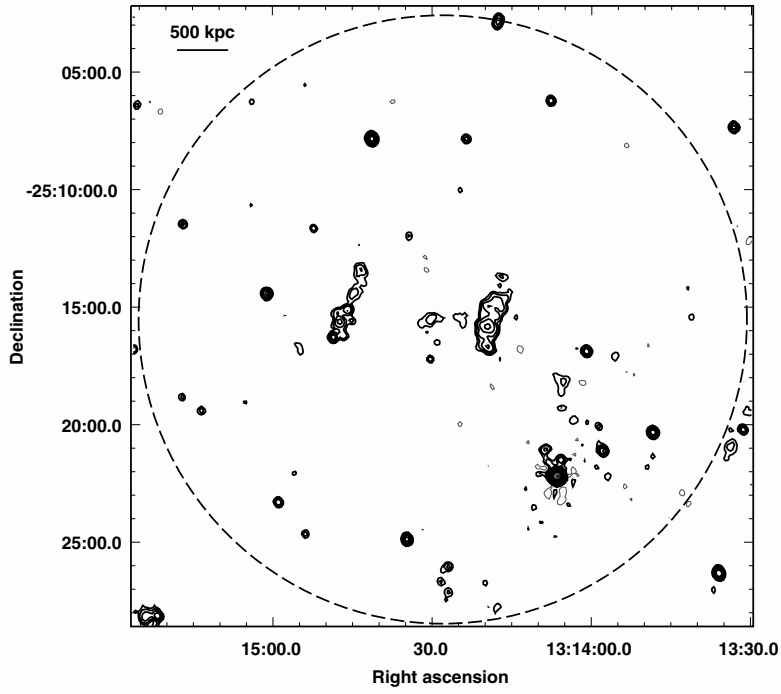

Fig. A.2. GMRT 610 MHz radio contours for the cluster RXCJ 1314.4–2515. The 1σ level in the image is 60 μJy b^{-1}. Contours are 0.3 × (±1, 2, 4, 8, 16...) mJy b^{-1}. The HPWB is 15.0″ × 13.0″, PA 15°. The radius of the dashed circle is the virial radius, corresponding to 12.94′ for this cluster.

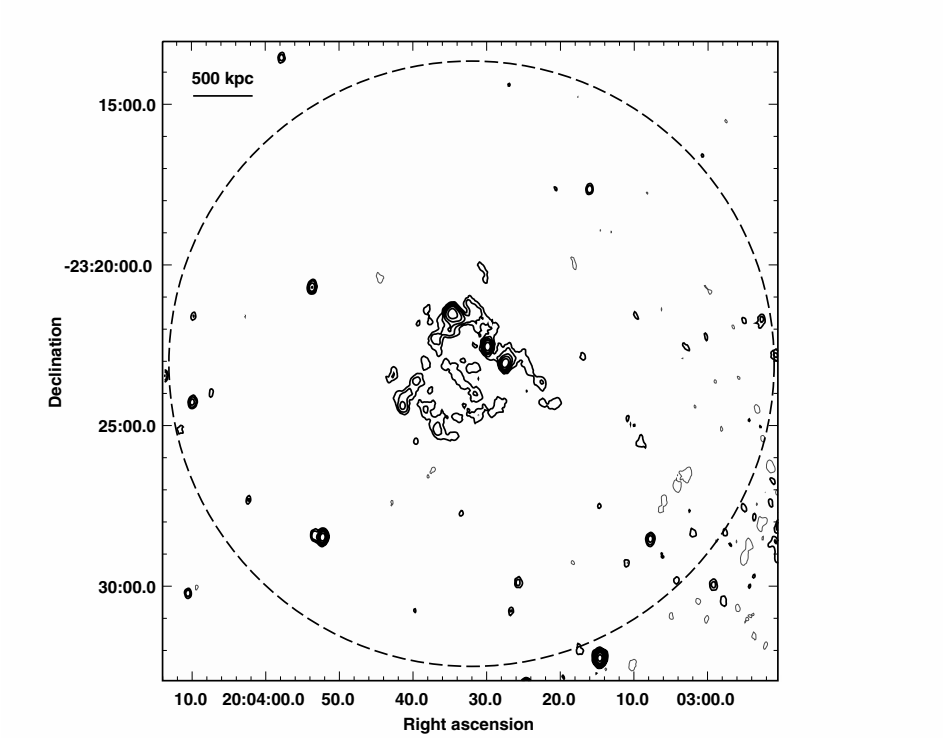

Fig. A.3. GMRT 610 MHz radio contours for the cluster RXCJ 2003.5–2323. The 1σ level in the image is 60 μJy b^{-1}. Contours are $0.3 \times (\pm 1, 2, 4, 8, 16...)$ mJy b^{-1}. The HPWB is $15.5'' \times 10.3''$, PA $-6°$. The radius of the dashed circle is the virial radius, corresponding to $9.91'$ for this cluster.

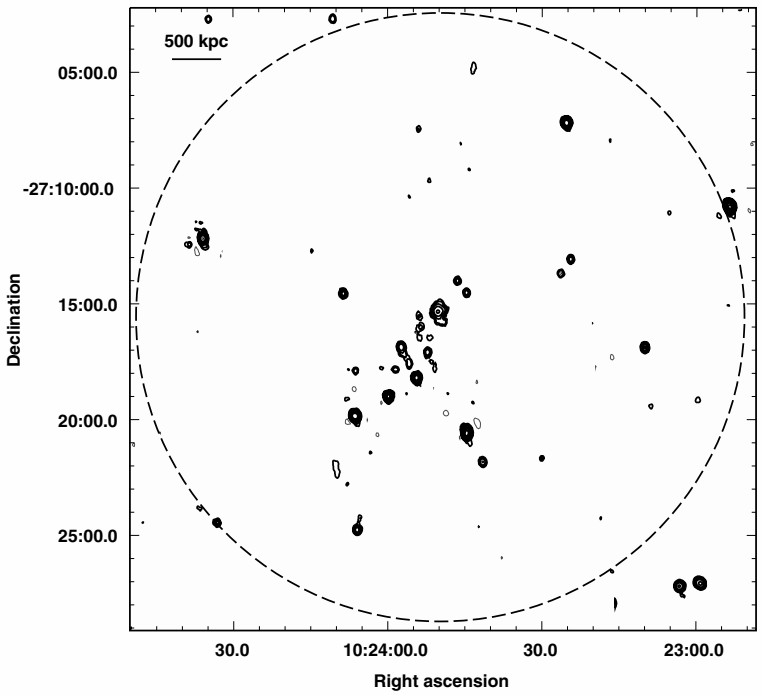

Fig. A.4. GMRT 610 MHz radio contours for the cluster A 3444. The 1σ level in the image is 60 μJy b^{-1}. Contours are $0.4 \times (\pm 1, 2, 4, 8, 16...)$ mJy b^{-1}. The HPWB is $15'' \times 12''$, PA $0°$. The radius of the dashed circle is the virial radius, corresponding to $13.14'$ for this cluster.

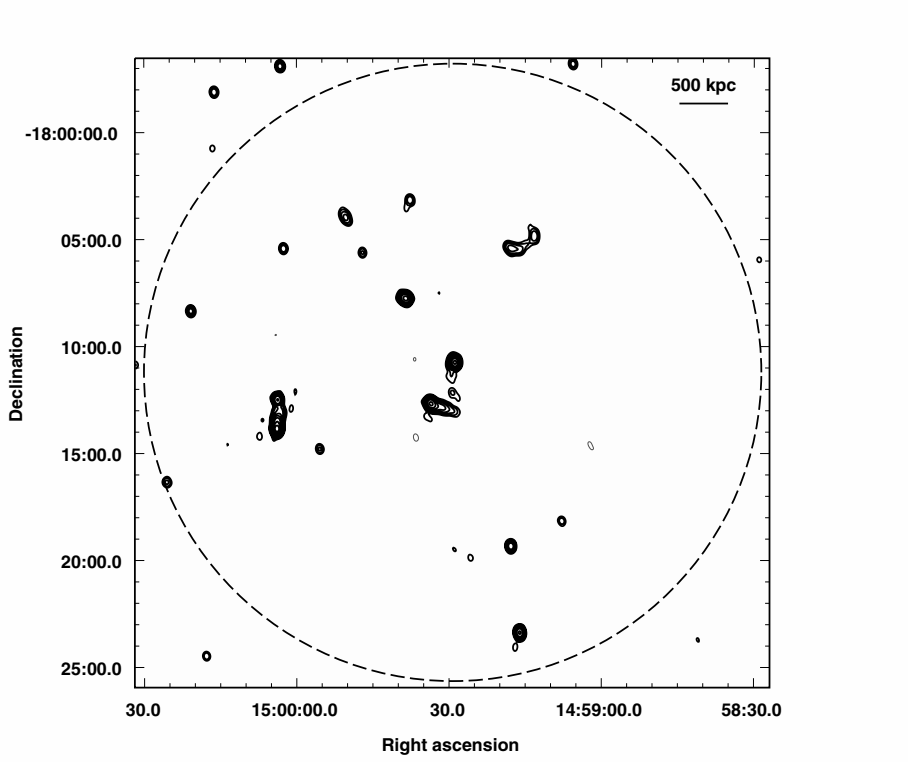

Fig. A.5. GMRT 610 MHz radio contours for the cluster S 780. The 1σ level in the image is 65 μJy b^{-1}. Contours are $0.3\times(\pm1, 2, 4, 8, 16...)$ mJy b^{-1}. The HPWB is $15'' \times 12''$, PA 0°. The radius of the inner circle is the virial radius, corresponding to 14.43′ for this cluster.

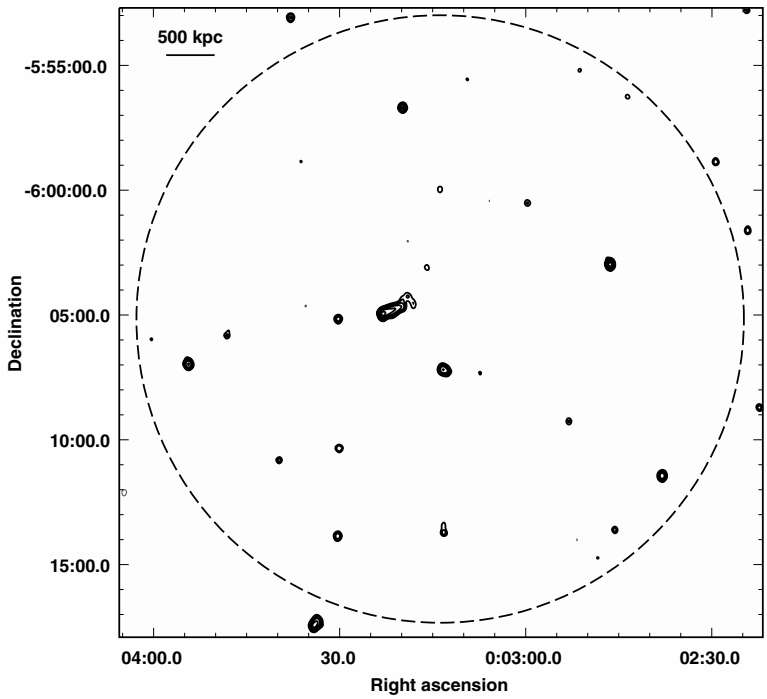

Fig. A.6. GMRT 610 MHz radio contours for the cluster A 2697. The 1σ level in the image is 80 μJy b^{-1}. Contours are $0.4 \times (\pm1, 2, 4, 8, 16...)$ mJy b^{-1}. The HPWB is $15'' \times 12''$, PA 0°. The radius of the dashed circle is the virial radius, corresponding to 12.17′ for this cluster.

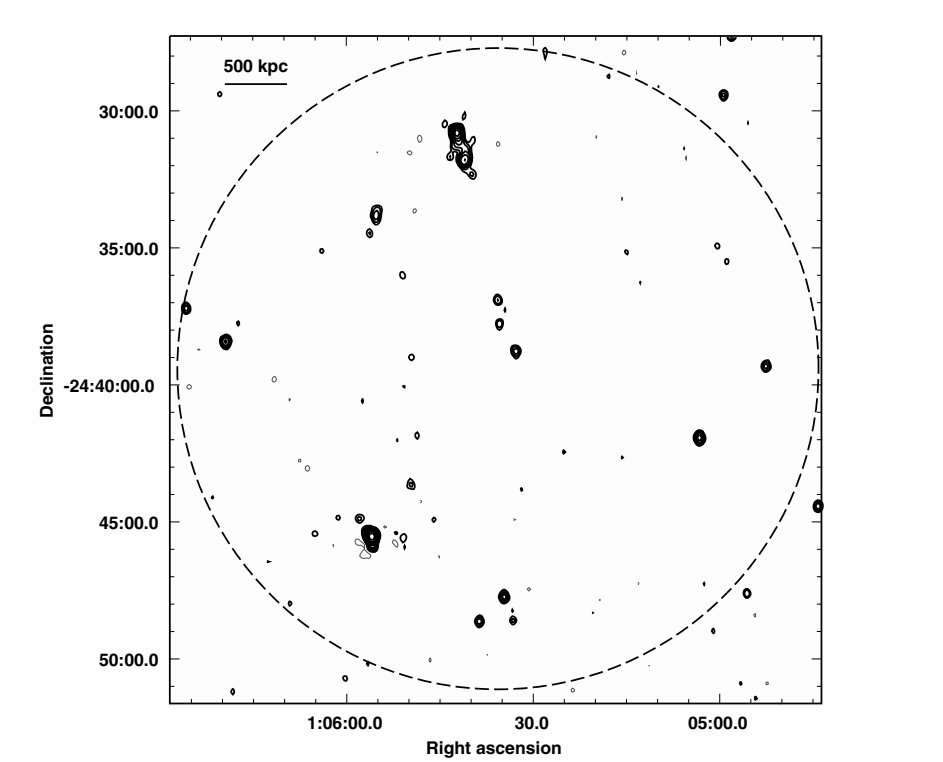

Fig. A.7. GMRT 610 MHz radio contours for the cluster A 141. The 1σ level in the image is 90 μJy b^{-1}. Contours are 0.45 × (±1, 2, 4, 8, 16...) mJy b^{-1}. The HPWB is 15″ × 12″, PA 0°. The radius of the dashed circle is the virial radius, corresponding to 11.79′ for this cluster.

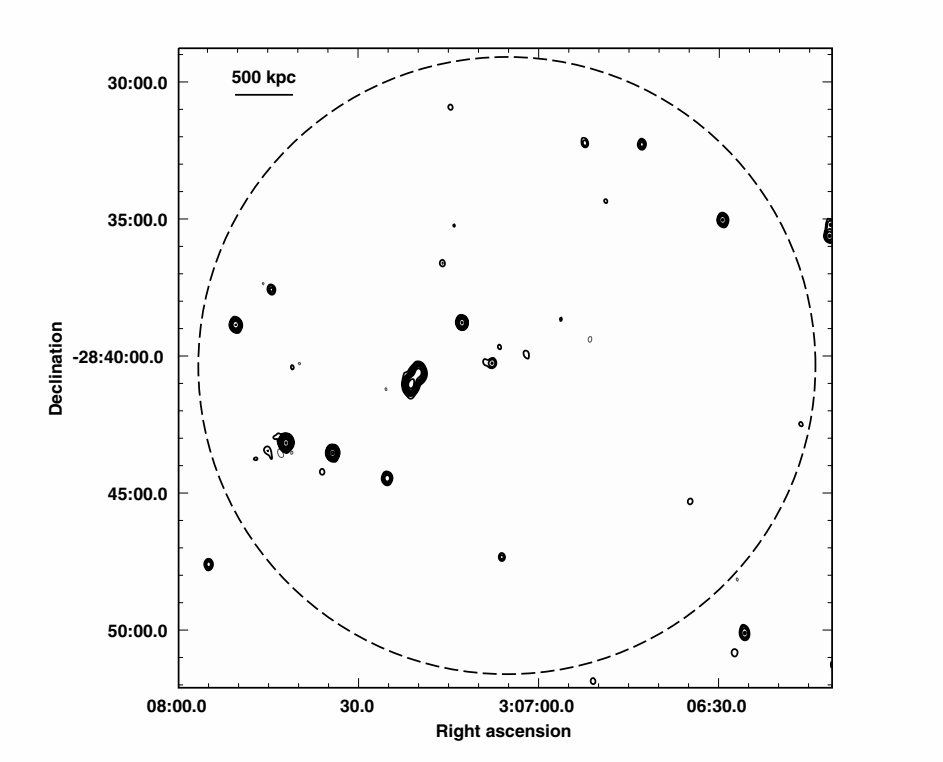

Fig. A.8. GMRT 610 MHz radio contours for the cluster A 3088. The 1σ level in the image is 65 μJy b^{-1}. Contours are 0.325 × (±1, 2, 4, 8, 16...) mJy b^{-1}. The HPWB is 15″ × 12″, PA 0°. The radius of the dashed circle is the virial radius, corresponding to 11.36′ for this cluster.

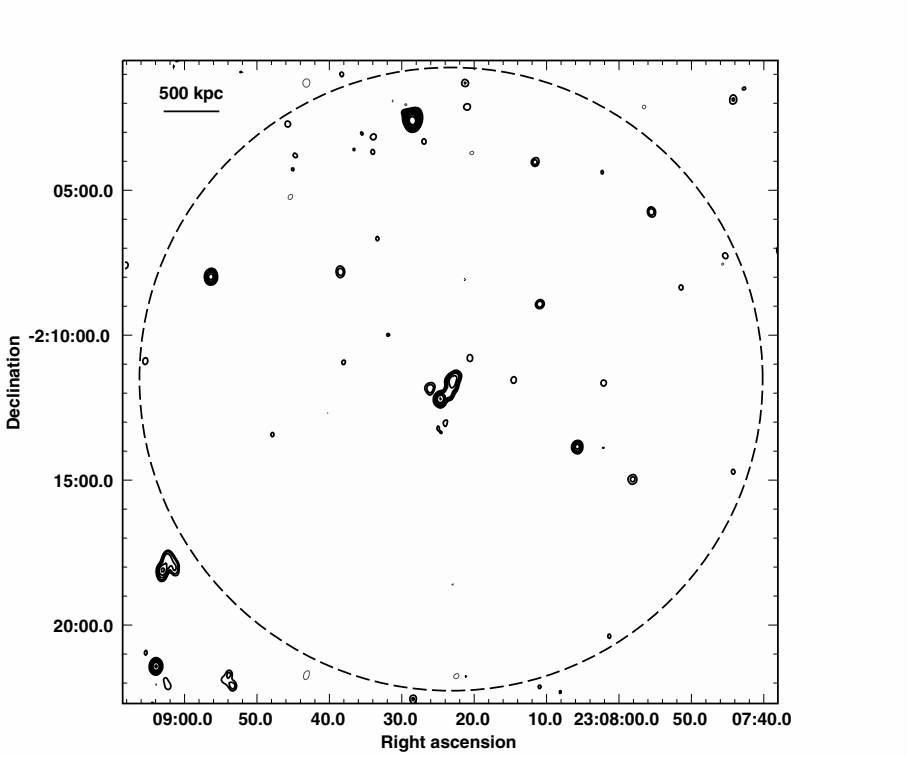

Fig. A.9. GMRT 610 MHz radio contours for the cluster A 2537. The 1σ level in the image is 80 μJy b^{-1}. Contours are 0.4 × (±1, 2, 4, 8, 16...) mJy b^{-1}. The HPWB is 15″ × 12″, PA 0°. The radius of the dashed circle is the virial radius, corresponding to 10.75′ for this cluster.

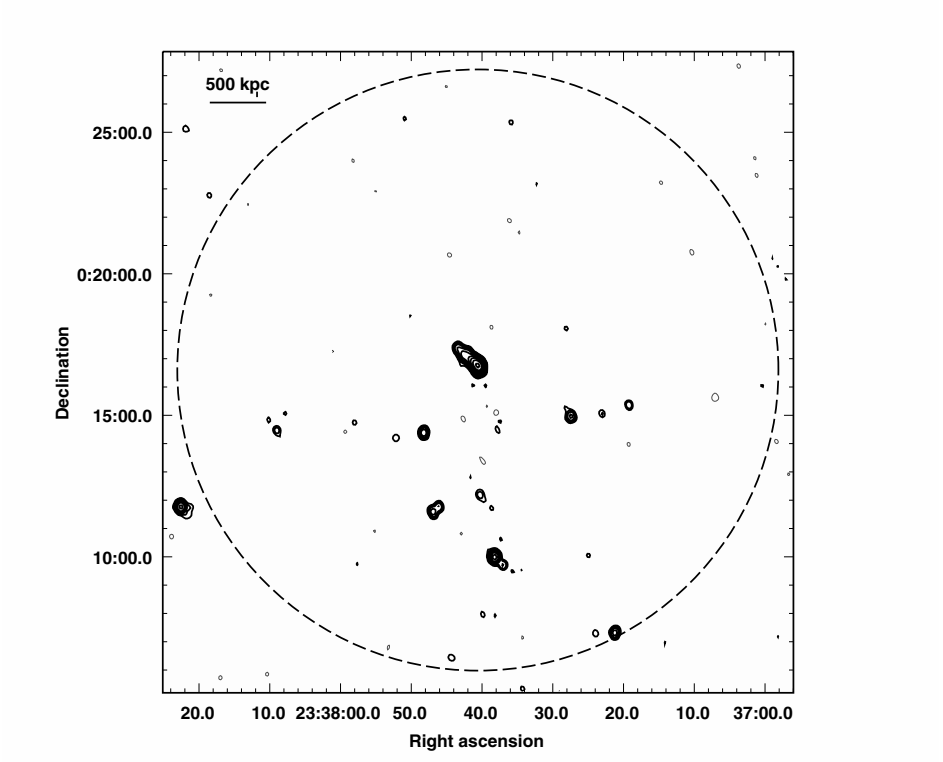

Fig. A.10. GMRT 610 MHz radio contours for the cluster A 2631. The 1σ level in the image is 80 μJy b^{-1}. Contours are 0.4 × (±1, 2, 4, 8, 16...) mJy b^{-1}. The HPWB is 15″ × 12″, PA 0°. The radius of the dashed circle is the virial radius, corresponding to 10.62′ for this cluster.